FACULTY OF SCIENCE

Estimating rooftop solar energy potential using spatial radiation models and thermal remote sensing: The case of Witwatersrand University

A research report Submitted to the Faculty of Science, University of the Witwatersrand, Johannesburg, in fulfilment of the requirements for the degree of Master of Science in Geographical Information Systems and Remote Sensing at the School of Geography, Archaeology & Environmental Studies.

NAME: RUDO HILDA NDEMERA

2526019

Supervisor

Professor Elhadi Adam

Co Supervisor: K. Ali Adem

March 2023

Declaration

I declare that this thesis is my own, unaided work. It is being submitted for the Msc in Geographical Information Systems and Remote Sensing research report at the University of the Witwatersrand, Johannesburg. It has not been submitted before for any degree or examination at any other university.

Signature:  Date: 21/09/23

ABSTRACT

The main purpose of this research was to estimate the University of Witwatersrand building's rooftop solar energy potential using the GIS-based solar Area Solar Radiation (ASR) analyst upward hemispherical view shed algorithm.

The two major datasets used in this research for rooftop solar energy potential modelling are building footprint data and the Digital Surface Model. Building footprint data, specifically rooftop area was extracted using machine learning CNTK unified toolkit and deep neural networks. The data was presented as individual polygon shape files for each building. The high-resolution Digital Surface Model imagery was sourced from the Advanced Land Observation Satellite. Pre-processing of the imagery was done for atmospheric correction. The DSM was then used in the Area Solar Radiation model to create an upward view shed for every point on the study area which is essential for computing solar radiation maps.

The efficiency of using this algorithm is that it considers the shading effects caused by surrounding topography and surrounding man-made features, alterations in the azimuth angle and the position of the sun. Apart from the incoming solar radiation reaching the rooftops, the elevation and orientation of the rooftop cells limit the solar panel tilt angle and intensity of the incoming solar radiation, respectively. These factors were used in setting the suitability criteria together with solar radiation for the identification of suitable rooftop cells in this research. The relationship between land surface temperature and solar radiation values was assessed to determine if it can be used as an indicator for solar panel efficiency.

Results from this research indicate that the University of Witwatersrand receives high levels of incoming solar radiation and has a high solar energy rooftop generation capacity that can meet the energy demand on campus. To improve accuracy of the research results, a drone could have been used to measure insolation across the study area to improve the spatial resolution. However, this was not possible due to various restrictions.

Acknowledgements

I would like to express my sincere gratitude to my supervisor, Professor Elhadi Adam, for his invaluable guidance and support throughout my master's programme. His expertise, patience and encouragement helped me to complete this research and the report.

I am very grateful to my colleagues and family for their support and love during this process. Without them, this journey would not have been possible.

TABLE OF CONTENTS

LIST OF FIGURES

LIST OF ACRONYMS

AHP	analytical hierarchical process
ALOS	Advanced Land Observation Satellite
ANN	artificial neural network
AOI	angle between sun and module
ASR	Area Solar Radiation
B	slope angle degree
DNI	direct normal irradiance
DSM	digital surface model
ELECTRE	Elimination and Choice Expressing Reality
ET	equation of time
G	actual solar radiation on PV
GDP	gross domestic product
HVAC	heating, ventilation and air conditioning
JAXA	Japanese Aerospace Exploration Agency
K	Boltzmann Constant
kWh/m^2	kilowatt hour per square meter
L8(OLI)	Landsat 8 (Operational Land Imager)
LST	land surface temperature
LT	local standard time
NDVI	Normalised Difference Vegetation Index
NPV	net present value
OLI	Operational Land Imager
PV	photovoltaic system
RMSE	root mean square error
SSA	spatial statistics analysis
ST	solar time
Ta	ambient temperature
TOA	top of atmosphere
UAS	Unnamed Aerial System
Vt	thermal voltage
Wits	University of Witwatersrand
WLC	weighted linear combination
WPM	weighted product method

CHAPTER ONE: GENERAL INTRODUCTION

Chapter 1 provides a general introduction explaining the current state of energy demand and supply globally. It describes the energy sectors in South Africa and their annual energy demand. The need and efforts to shift to renewable energy sources, in particular solar energy, are highlighted in reference to the current crisis at the university. Motivation for the research was also explained together with conclusions and recommendations for future related studies.

1.1 Introduction

Recently, the magnitude and nature of global energy demand has increased in an unprecedented manner as a consequence of the rapid growth of population and modernisation (T.Soares, 2019). From the 18th century to the 19th century (that is, during the Industrial Revolution) and beyond, the extensive use of conventional fossil fuels has led to the emission of greenhouse gases (including methane and carbon dioxide). This has resulted in a rapid increase in the earth's average atmospheric temperature and other adverse environmental concerns (T.Soares 2019). Green/renewable forms of energy are being used as alternative energy sources and have proved their capacity to meet the growing energy demand. These are readily available compared to non-renewable energy which is depleted over time. They also provide a relatively clean form of energy. Diversifying energy sources using renewable energy has positive effects on the economy by reducing imported fuel dependency (Kuma et al, 2018).

Energy demand varies by sector globally and the three main drivers of the demand are technology, policy and consumer preferences. New technology allows for the reduced consumption of energy through the designing of energy-efficient appliances. Consistent government policies stimulate new technologies and influence consumer choices (T.Soares, 2019). Global energy consumption sectors are divided into residential, commercial, industrial, transportation and electricity generation (Singh et al., 2013). Industrial sectors use the most electricity (as they support the building and construction of infrastructure and manufacturing of products). These are followed by transportation (owing to the need to move goods and for personal mobility). Residential and communication sectors consume the least electricity.

In South Africa, there are five energy consumption sectors namely, agricultural, industrial, transport, residential and commercial sectors (Menyah & Wolde-Rufael, 2010). Statistics from the Department of Energy indicate that the manufacturing industry consumes an annual average of 70% of the total generated energy while the transport sector consumes 13.5%. South Africa has a high solar energy generation potential, one of the highest in the world receiving above

2500 hours of sunshine annually (P. Menyah,2010). The South African renewable energy programme resulted in the establishment of a solar PV project in 2013 which is now supplying 5 423 megawatts to the Eskom national grid – which is about 7% of the total energy produced in the country (Ritchi, 2023) The ongoing energy crisis in South Africa has led to the decline of economic growth and disruption of the provision of social services (for example water and sanitation). Load shedding has hindered economic growth by 10% (Stofberg, 2022), which has led to a decline in investment prospects.

Solar energy reaches the earth's surface as electromagnetic radiation comprised of photons. Irradiation reaching a particular location at the earth's surface at a specific time interval and fluctuates according to local, spatial, global, temporal and meteorological factors). Indicators of high solar energy include high evaporation rates resulting in precipitation, thereby providing hydropower, photosynthesis rate and wind caused by heated air masses. When selecting the optimal location for positioning solar panels, it is crucial to accurately model the annual, monthly and daily global radiation reaching the earth's surface This ensures the appropriate positioning of solar panels at sights with the greatest electricity generation potential.

Remote sensing technology is being utilised to model solar radiation potential due to its ability to generate efficient results in a timely and cost-effective manner. Within the last two decades, notable progress was made towards the development of solar radiation models using artificial intelligence techniques, and analytical and statistical simulations and these include models developed by, (Mubiru and Banda ,2008), (Adrian et al. 2001) and (Pescador, 2005). These models usually require empirically determined parameters that pose a challenge where measurement instruments are not available. Moreover, the empirical models assume that ground truth data follows specific patterns although location-specific data differs between each building. This results in long-term solar potential modelling bias for areas with missing data/where ground data cannot be measured. To curb this problem, spatial interpolation methods based on inverse distance weighting and spatial autocorrelation have been implemented.

In regions where solar radiation data is available, Artificial Neural Network (ANN) is used for performing data training while testing is done in regions where data is not available. Other input values used in training which affect solar radiation include the average temperature, sunshine duration, wind speed, longitude, latitude and precipitation (Horfieka,2004). The

accuracy of the ANN is increased by using a multi-regression analysis and genetic algorithm to model monthly average daily solar radiation for regions without solar radiation values.

GIS is being implemented in the mapping of diverse spatial and temporal scales of renewable energy distribution systems (Taskin Jamal, 2002). GIS-based models have been developed including the advanced model for biological and ecological applications by (Fu and Rich 2000), which is presented as an Environmental Systems Research Institute's ArcMap extension (Solar Radiation Toolset). This model is the basis of the methodology proposed in this research. It computes an upward-facing hemispherical viewshed based on a digital surface mode and is suitable for modelling using high spatial resolution input data. Another GIS-based model is the SRAD which is suitable for modelling of meso- and top-scale processes across the landscape. Unfortunately, the calculation of solar radiation over large areas is limited in this model. Another GIS-based radiation model is the r.sun which computes beam diffusion and the reflected energy of the global radiation across clear and overcast skies (Hofierka, 2002). This method is suitable for modelling across large areas and contains a shadowing algorithm which considers shadowing effects.

Solar radiation maps have also been computed in the form of spatial databases. These do not perform a direct measurement of solar radiation but use existing solar radiation maps to simulate the annual sunshine hours across regions. The accuracy of these models is verified by comparing the solar radiation values to ground data, for example global horizontal irradiance (GHI) and diffuse horizontal irradiance (DHI).

The ongoing energy crisis has resulted in the disruption of campus systems during load shedding. This negatively affects academic progress for students. To avoid this, there is need to explore alternative energy sources to ensure that power supply is not interrupted during load shedding. Conducting solar energy potential research at the University of Witwatersrand also provides a valuable contribution to the institution in its efforts to gradually shift to renewable energy sources which are more affordable and reduce carbon emissions. This research also provides crucial information needed in economic feasibility analysis for solar panel installation, for example total suitable rooftop area and expected energy output per square meter which is needed for sound decision making.

1.1 Scope of study

This study focuses on modelling solar radiation across the University of Witwatersrand, a study area which covers a relatively small area spatial extent. The view shed boundary of the study area is limited to east and west campus buildings. This is because the algorithm is computationally intensive hence it is important to limit the spatial extent to the study area. Solar radiation values within the study area do not differ from those recorded over extensive areas (at regional level). However, distribution of solar radiation on the campus rooftops is heterogonous which can be attributed to presence of obstructions due to variation of the buildings' heights and other physical obstructions. This research explored variation of insolation between summer and winter months to investigate seasonal trends. Daily variations in solar energy distribution were also modelled to identify the daily trends for solar radiation distribution across campus.

1.2 Problem statement

This study addresses the ongoing energy crisis at the University of Witwatersrand caused by national load-shedding. It presents a method for exploring the university's rooftop solar energy potential through use of Geographical Information Systems and Remote Sensing. This method was preferred as it allows for timely integration and analysis of several factors which influence solar energy potential.

South Africa has suffered rolling blackouts with the existing infrastructure failing to keep up with energy demands, leading to the destabilisation of the energy grid. Currently, the use of diesel generators has managed to ease the impact of load-shedding across the Wits campuses. However, these generators frequently break down as they are not designed to operate for prolonged periods. A pilot project involved the installation of photovoltaic systems at Goldfields Lab, Construction Economics and Management, Origins Centre, Commerce Law and Management, FAB and Robert Sobukwe Building (J.Huang, 2022).

The university has experienced the loss of heating and cooling in lecture rooms and residences, disruption of science lab experiments and loss of internet services among other challenges during load shedding. However, the use of generators is not sustainable owing to the high fuel costs (R50000 to R140000) per hour. To add on, they emit particulate matter (including benzene, arsenic and formaldehyde), which all pose environmental and health risks.

Based on these challenges, the university needs to introduce renewable energy sources to reduce dependence on the national grid. This study set out to identify buildings with suitable rooftops for installation of rooftop solar panels and their electricity generation capacity.

1.3 Aim and objectives

Aim: Determine rooftop solar energy potential using GIS based spatial radiation models.

Objectives:

- Modelling of daily and monthly local variations of incoming solar radiation across campus buildings rooftops.
- Perform rooftop suitability analysis based on rooftops falling within the following criteria: 90◦ slope, orientation of North facing roofs and output power potential above 0.26 kWh/m^2.
- Determine daily local variations of LST and determine its relationship with solar radiation.
- Calculate power output per building based on rooftop area and energy generated per square meter.

.

CHAPTER TWO: LITERATURE REVIEW

Chapter introduction: This chapter explains the contribution of solar energy to climate change mitigation and the current state of energy consumption in South Africa's commercial sector. It also states the factors which affect solar radiation distribution which were considered in this study and their significance based on previous research. The framework guiding the research is introduced together with its past achievements, limitations and possible recommendations for future work. Lastly, the methods used in this research for identification of suitable rooftops for installation of solar panels are discussed.

2.1 Contribution of solar energy to climate change mitigation

The demand for energy to meet economic and social services is increasing. Since 1850, the global use of fossil fuels has increased greatly and has dominated the energy supply, which has led to rapid growth in carbon dioxide emissions. Carbon dioxide concentration in the atmosphere has increased by 39% above pre-industrial levels (V. Kray et al., 2016). Greenhouse gas emissions resulting from the provision of energy services has contributed significantly (57%) to the increase in greenhouse gas concentration in the atmosphere (Keles et al., 2012). The Intergovernmental Panel on Climate Change (IPCC) assessment report reviewed that the observed increase in global temperatures since the mid-18th century is attributed to the increase in anthropogenic greenhouse gas concentrations. The use of non-renewable energy sources directly contributes to climate change, which is a serious threat to the environment. Extreme weather conditions caused by rising temperatures include droughts, melting polar ice leading to floods, storms and wildfires among other disasters.

South Africa depends on its abundant coal resources for electricity generation. 90% of the country's power is generated from coal. Statistics from the Energy Information Administration revealed that South Africa is the 6th largest producer of coal globally and has the highest carbon emission, making up 42% of the emissions in Africa. Amid efforts to reduce these emissions, South Africa became one of the Kyoto Protocol and Paris Agreement signatories with a target of reducing emissions by 34% in 2020.

Solar energy is one of the most relied-on technologies for climate change mitigation owing to its long-term availability and low carbon emission. The sun is the major source of energy available on earth. Biomass, hydropower, wind power and fossil fuels trace their energy source back to the sun. Solar radiation is constantly available on earth, about 62 000 terawatts annually

(Daukes et al., 2009). This greatly exceeds the worldwide annual average power consumption of 16 terawatts. 86.5% of this energy is generated from fossil fuels. Fossil fuels adversely affect the environment through the emission of carbon dioxide, CFCs and methane. These greenhouse gases drive thermal changes through the absorption of infrared energy which leads to rising global temperatures. This causes heat waves, droughts, floods and wildfires among other disasters. A new energy paradigm based on local renewable energies is needed, and this will contribute to a reduction of greenhouse gas emissions and climate change mitigation (Soares, 2019).

In terms of greenhouse gas emissions, energy from solar systems is ranked as one of the lowest carbon energy technology. To reduce carbon emissions, there is a need to install large numbers of concentrated solar power systems globally. If early investment is made in future and existing solar technology, the International Energy Agency indicates that solar energy can contribute to 11% of the global energy supply by 2050.

Currently, the use of solar energy has grown by approximately 40% over the last 10 years (V. Kray et al 2016 et al., 2014). (Tuekenburg et al. 2012) estimated the global technical potential of solar energy to range from 160EJ/year to 50 000EJ/year. However, the shift to solar energy will require the active involvement of government policymakers and the reduction of renewable energy technologies. Gradually, policies may be implemented to lower the use of fossil fuels by increasing their prices.

2.2 Energy crisis in South Africa and the need for renewable energy alternatives

Since 2022, Eskom has been unable to meet the country's electricity demand, and this has resulted in unprecedented load shedding. The ongoing energy crisis has been attributed to several factors including delays in upgrading the Koeberg nuclear power station, obsolete coal power systems and significant breakdowns at the Kusile and Medupi coal power stations. South Africa's economy relies on coal and low-cost electricity to power the mining and metal processing industry. Anglo America Platinum is one of the mines which was affected by load-shedding. It is reported that night shift operations were suspended for the safety of the workers, and this resulted in significant economic losses. The energy sector contributes 15% of the gross domestic product (Keles, 2018). The imminent depletion of coal reserves and obsolete nature of generation equipment poses a threat to the economy. Energy demand is projected to increase in the next 50 years; hence it is necessary to invest in renewable energy sources. In 2022,

Eskom energy tariffs increased by 18.65%, which indicates the utility's failure to meet the country's energy demand (Patrick, 2022).

Information from the Gauteng City Regional Observatory survey revealed that between 2013 and 2014, the number of residents who had access to wind/solar energy increased from 0.8 to 5%. Residents who reported having access to generators increased from 0.3% to 4% between 2014 and 2021. Hydropower only contributes 1.4% of the total energy supply. This indicates that solar energy is the most explored renewable energy source based on its affordability. To reduce South Africa's economic vulnerability to the escalating cost of imported fuels, there is a need to gradually shift to renewable energy alternatives. Employment creation and reduction of economic/energy vulnerability are some of the advantages resulting from renewable energy exploration. Renewable energy sources require lower maintenance costs and result in increased national energy security. Eskom generation operations emit carbon dioxide levels above the permitted threshold (Crompton, 2022).

2.3 Current state of energy consumption in the commercial sector

South Africa's electricity needs are expected to be more than 56 000 MWh by 2030 according to the country's Department of Energy (Mokoena, 2021). The Department indicates that the commercial sector consumes the least energy (less than 15%) as compared to other sectors and is mainly associated with heating and cooling of buildings (Ritchie m, 2020). Educational institutions, service businesses, hospitals and other government facilities are classified under the commercial sector. Despite financial constraints, electricity usage in South Africa's educational institutions remains unchecked. According to the 2019 South Africa Energy Report, South Africa has 23 471 public schools whose estimated usage is 3.5 terawatts per hour annually, which yields a generation cost of R 330 million (Ritchie, 2023). Every school is expected to use well over 52 kWh per day, which contributes to 3.5% of total electricity consumption daily.

The University of Witwatersrand uses about 60 GWh a year (J.Huang, 2022). Water heating in hostels, catering services and air conditioning systems consume the most energy. Energy is also required for offices and lecture room lighting, security systems and lab experiments among other uses. An energy efficiency programme was launched in 2017 to introduce renewable energy alternatives, specifically photovoltaic systems and to eliminate dependence on the national grid (Huang, 2022).

2.4 Framework for solar radiation modelling

In this research, the ArcGIS ASR model (Solar analyst) was used for solar energy potential modelling. The method uses high-resolution DSM data together with the upward-looking hemispherical viewshed algorithm to analyse the variables that influence solar radiation potential for each building. The total amount of incoming solar radiation calculated for a particular location or area is given as the sum of diffuse and direct radiation. The calculation of global, diffuse and direct radiation is repeated for each location on the topographic surface, producing solar radiation maps for the study area. The solar analyst module is also efficient owing to its ability to produce accurate and versatile maps promptly. The model is available in open-source GIS applications which provides easy access to end users. It also allows for sensitivity analysis to be carried out to assess the effects of adjusting specific input parameters which affect solar radiation.

This spatial radiation model has been used in published literature (Clifton and Boruff, 2010; Gastli and Charabi, 2010) and has proved to be relatively fast and accurate in the modelling of solar radiation. Solar radiation can be set to any temporal resolution in the solar analyst which is crucial to this research since it explores daily and monthly trends. The model accounts for daily and seasonal shifts in the angle of the sun, atmospheric effects, elevation, steepness, aspect and effects of shadows caused by surrounding topography. Apart from physical parameters, the model requires building footprint data for example height, rooftop area and floor area ratio to compute solar energy potential (Guo et al.2020). This results in the need to analyse both physical and technical solar energy potential simultaneously to achieve accurate applicable results related to power generation. In a study carried out in India, (J. Melius,2013), the physical solar energy potential assessment was done through using the hemispherical view shed algorithm to create and analyse solar radiation maps paying special attention to the impact of urban morphology on shading. Like this research, the technical assessment involved the calculation of solar power generation potential based on rooftop area and the efficiency of type of solar panels to be installed. The major drawback observed in this study was that the model did not model cloud type, thickness and cloud distribution. This is because clouds are difficult to model as information is not available in all areas. In a study by (Kaleshwarwar,2023) the hemispherical view shed was used to assess solar energy potential in India, Nagpur, and results indicated that there was little variation on average annual solar radiation since all the buildings are in the same vicinity, solar energy potential was mostly affected by variation of rooftop area and other building characteristics rather than availability of irradiance. This resembles results from this

research which indicates the suitability of this algorithm's applicability over small study areas. The study also revealed a correlation of 100% between solar energy potential and rooftop area. This is consistent with previous findings (W. Gun et al., 2019) stating that an increase or decrease in rooftop area directly affects solar energy generation potential.

Most of the methods which perform solar radiation simulations account for the rooftops and the complexity of the terrain based on implementation of GIS and digital surface models from various sources. These sources include satellite imagery, Unnamed Aerial Vehicles and Lidar data. In this study, the Advanced Land Observation Satellite (ALOS-4) imagery was used as the input into the solar radiation model. The remotely sensed DSM was combined with shape files showing building footprint data representing each building's rooftop and surface area. However, the 10m spatial resolution was relatively low which may impact accuracy of the research results. Other recent studies have incorporated the use of LIDAR data as an input into the solar analyst model. Acquisition of 3D high resolution DSM imagery is costly which is one of the major challenges associated with this simulation model. Brito et al,2019 conducted a research to model solar energy potential for Libson and used Lidar data as an input in the model. High resolution results were produced showing fully identified buildings, roofs and $1m^2$ elements of facades. The results were validated by comparing experimental results of photovoltaic output on a south facing surface in a summer and winter month. There was a reasonable correlation between modelled and measured values which indicates the efficiency of the model. One of the recommendations from this research is to extend the validation sites to other locations with different urban layouts. The results could also be improved by integrating the model with another detailed PV model adding an extra data layer for visualisation to allow the display of rooftop electricity generation potential. Moreover, Hourly radiation data was generated but could not be visualised as this required massive additional data. In a research by (Quispe, 2023), estimation of rooftop photovoltaic potential in Calabar, Nigeria was done using this study's framework. Apart from the suitability of rooftop solar energy potential, the results revealed that regions with dense buildings indicate high potential for photovoltaic systems as compared to regions where buildings are sparsely distributed. This is an important aspect which has not been analysed in previous solar energy potential studies. In a study done in 2022 at the National University of Science and Technology (E. Maboob et al, 2022), solar radiation maps were successfully developed using the area solar radiation model. The results showed the spatial distribution of solar radiation across the university which is an important contribution in the solar panel installation site selection process. The solar

radiation modelling was based on the topographic aspects of the study area and did not account for individual rooftop modelling. This indicates the flexibility of the model for use in modelling solar radiation where high resolution digital surface model imagery is not available.

2.5 Factors affecting solar radiation distribution

When developing solar installations, numerous factors which affect solar radiation distribution are taken into consideration. These can be categorised into technical, political, environmental and economic factors. The main factors considered by previous studies for solar panel installation site selection include slope, aspect, weather conditions, and distance to power lines, sand/dust risk, access to water, LULC profiles and supply-demand balance. This research focused on the geophysical factors which affect rooftop solar energy distribution, and these are discussed below.

2.5.1 The impact of shadowing, orientation and tilt angle on solar radiation distribution

Surface orientation, surrounding obstacles and gradient all have a significant effect on the performance of photovoltaic panel systems as they contribute to shadowing (Carrion et al., 2007). The shadowing effect occurs when solar panels do not receive the same amount of irradiation level throughout the system owing to surrounding obstacles. Partial shading on one cell significantly reduces the power output of the system. In this case, the cells receiving lower irradiance absorb power instead of producing it. This is usually solved by using micro invertors or bypass diodes (Keles, 2012).

The determination of appropriate orientation varies with the location under study. The relative angular position of the sun, daily, monthly or annually determines the orientation for maximum solar generation. Solar panels must always face the direction of the sun so that the incident light is perpendicular to the module. In the southern hemisphere, north-facing locations receive the maximum sunlight annually, while in the northern hemisphere, south-facing slopes receive maximum (L. Pratson, 2011) Because of this, northern hemisphere installations should follow a southern orientation exposure to obtain the highest radiation intensity in general and the reverse is true in the southern hemisphere. The mounting panels on movable stands have proved to be efficient as panels can be automatically adjusted to the optimum angle at a specific time of the day (V. Krey 2016).

In research conducted by Carrion et al. (2007), the importance of gradient in the analysis of suitable locations for solar panel installation was explored in Andalusia. Results from the

research indicated that sites within a slope of 2% experience shadowing effects owing to the solar panels themselves. In another similar study by Charabi and Gastli (2011), even slopes of >5% resulted in shadow effects. This is experienced especially where installations involve multiple rows of solar panels. A maximum of 7% slope overcame the shadowing effect in a study by Bravo (2007). Surrounding obstacles greatly reduce the exposure of solar panels. In this research, the variation of building height results in obscuring of affected rooftop cells resulting in shading. Because of this, only unshaded areas should be designated as suitable.

Tilt angle has been widely considered a major factor affecting solar panel efficiency. Climatic conditions and geographic latitude influence the determination of the tilt angle. The optimum tilt angle of a photovoltaic array should be equivalent to latitude with an azimuth due south in the northern hemisphere annually (Rowlands et al., 2011). Various simulation software such as PVsyst and TRNSYS have been used in several studies (for example, Cheng et al., 2009; Hussein et al., 2004) to determine optimal tilt angle. These models consider the cloud clearness index, geographic location, diffuse and global irradiation and other parameters (Soares 2019

Marcos (1994) states that the optimum angle varies daily – hence changing the orientation daily is impractical. For this reason, he suggested that average seasonal angles should be fixed and calculated as 'value of latitude' angle +/−15°; this angle was incorporated in research by (Gunerhan ,2007). These results are like those in other studies, including the work of Calabro (2009) whose simulation optimum tilt angle for Chiayi, Taiwan was 20 degrees. This method was used to identify the optimum tilt angle in this study.

However, (Popp, 2011) introduced a different finding. His research highlighted that most optimum tilt angle models do not consider cell temperature effects and surface reflection characteristics done using short circuit current and measuring open circuit voltage and temperature cell to find the optimum tilt angle in Hannover, Germany. Results demonstrate that there was a difference of only 6% between winter and summer values for optimum tilt angles. This indicates that differences are much smaller as compared to those obtained from modelled results. This can be explained by the effects of temperature or inaccuracies of the model.

2.5.2 Direct normal irradiation

The main resource for solar panel technology is direct normal irradiance (DNI). This is the amount of solar radiation at the surface of the earth on a flat surface perpendicular to the sun's beam with surrounding diffuse sky radiation (NASA ASDC, 2009). This is equivalent to the

solar constant minus atmospheric losses due to absorption and scattering. Unlike some other forms of solar power, which can utilise both diffuse and direct solar irradiance, concentrated solar systems only utilise direct irradiance component and is best suited to locations with high annual direct normal irradiation. While solar systems can technically operate at levels as low as 1800 kWh/m^2 annually, the generally accepted minimum for commercial CSP projects is 2000+ kWh/m^2 annually Elevation, slope, daily seasonal shifts and shadowing effects from surrounding topography all influence and are all incorporated in the solar analyst module used in this study.

While solar panels are generally preferred because of their clean nature, construction processes for the installation of PV systems may result in significant environmental harm to the selected site. Environmental protection laws must be adhered to, to avoid violation during the site selection process. To add on, water resources are required for the cleaning and cooling of any other solar system components. It would be economic to install the panels at a tilt angle which allows self-cleaning when it rains. Nanotech technology solutions are an alternative solution as they provide nonstick coating, reducing the need for cleaning. Visual and construction impacts on the local community must be considered to maintain an aesthetically pleasing view.

Research conducted by Carrion et al. (2007) considered the energy losses to transmission, together with the distance of substations to solar installation systems. This energy loss from transmission over distance is a direct economic loss; hence in other scenarios, it is considered the most important factor in solar panel site selection. However, the distance is defined differently in various scopes of interest.

2.6 Decision support for identification of suitable rooftop area

In the 1970s, energy generation policies were formed towards models for exploring the energy economic relationships in the energy sector (Pohekar, 2004). As time progressed environmental awareness grew and this slightly altered the decision framework. Multi-criteria approaches have increasingly become necessary due to the need to incorporate environmental, political, social and technological considerations in energy planning. Multi-criteria analysis enables decision-makers to identify explicitly, efficient and rational choices (Haurant et al., 2011). These methods simplify the progress of decision-making where there are multiple objectives. Usually, the objectives are conflicting, and the desired results depend on the decision-makers/stakeholders. Multi-criteria decision analysis is mainly based on priority setting and outranking to achieve the desired income. In this research, the identification of data layers

which directly influence solar radiation was done and they were overlaid to identify rooftop cells fitting within the combination of the suitable criteria. Specific conditions for each layer are set in this case, north facing slope of value between 60^0 to 90^0 and above-average output solar power generation potential per building. The cells which fall within this criterion are assigned to the 'suitable' condition unit while those which are not in this criterion are assigned to the 'unsuitable' condition unit. This method is appropriate for this research as it requires a limited number of factors for site suitability analysis (Aldo, 2006)

Chapter Conclusion: The framework presents a method to analyse solar energy potential in a fast, efficient and cost-effective way. The method is transferrable and can be used for any area where DSM/DEM data is available. Previous studies have seen the successful applicability of the model across both large- and small-scale study areas. However, results are mostly accurate with the use of high-resolution 3D DSM imagery which is expensive to acquire. Results from solar radiation models need to be validated against ground data from measuring instruments, solar energy generation information from home-based PV systems and information from other relevant local authorities which has not been done in most studies. Gaps arising from this research include the lack of other criteria to determine suitability of solar panels installation, for example economic and social aspects. Moreover, building height was not accounted for in the model. However, a visual assessment to check for obstructions due to building height was done manually during a ground survey.

CHAPTER THREE: METHODOLOGY

Chapter 3 gives a brief description of the study area and its climatic conditions in relation to solar radiation trends. It also explains the sources and processes involved in the acquisition of the remotely sensed data used in this study. A detailed explanation of the relevance of the data including spatial and temporal resolution is provided. The steps involved in the suitability analysis are outlined. Data analysis and validation approaches are explained.

3.1 Remote sensing data acquisition and pre-processing

3.1.1 Acquisition of Digital Surface Model imagery

The solar radiation model requires the study area Digital Surface Model (DSM) as the main input. The DSM was obtained from the Advanced Land Observation Satellite 4 (ALOS -4) and has a relatively high spatial resolution of 13 m*13 m. The DSM is compiled from images collected by a panchromatic remote sensing instrument managed by the Japanese Aerospace Exploration Agency (JAXA). The major advantage of this platform is that it provides open-source high-resolution 3D DSMs at a global scale – the only platform to do so.

This global dataset was updated in May 2021 with void filling done using data from the STRM (Space Shuttle Radar Topography) and ASTER (Advanced Space borne Thermal Emission and Reflection Radiometer) digital elevation model imagery. This makes the dataset relevant to this research because no major changes in the DSM are expected since the study area is geomorphically stable owing to its built-up nature. Further, the focus is on the building rooftops whose elevation values are relatively constant. This implies that the same DSM can be used for different time configurations for the three years under observation in this study.

3.1.2 Landsat 8 Operational Land Imager: Retrieval of land surface temperature

To derive LST, Landsat 8 (B10 and B11) Operational Land Imagery was used, and the algorithm is described in Figure 2. Although the resolution is coarse (30 m * 30 m), this was the best choice given the fact that it has the highest resolution in thermal infrared bands compared to other open-source satellites. This satellite has advanced technology that applies quantum physics to detect heat. Its spectral resolution covers the TIRS (Thermal Infrared Sensor) bands needed for calculation of LST. The temporal resolution of Landsat 8 is 16 days which suffices for monthly modelling of LST for the three years under study. Based on the

USGS (United States Geological Survey) website, the difference between the ground-based results and the TIRS is a maximum of 5 Kelvin, although this varies across seasons.

3.1.3 Building footprint data

The rooftop area for each of the buildings was extracted using CNTK Unified Toolkit and deep neural networks to outline building footprints from satellite imagery. To ensure the best output, suspicious noise (false positives) and data are removed from the predictions. A polygonisation algorithm was used to detect the building angles and edges to create the building rooftop outline which can be accessed as a shapefile. Validation to assess the algorithm found it was found to have 99.3% precision (Haris, 2020). However, manual correction was applied to 12 buildings whose footprints overlapped. Ground truthing was done by comparing satellite imagery to East and West Campus buildings to avoid any omissions.

3.2 Study area

The study area where the research was based was, the University of Witwatersrand (see Figure 1). This is a South African public research university located in the north-central part of Johannesburg, Braamfontein (26° 11′ 28″ S, 28° 2′ 16″ E). Braamfontein land use is largely commercial and residential. This region is characterized by a subtropical climate, experiencing humid and hot summers with an average maximum temperature of 26 °C and a minimum of 4 °C annually.

Figure 1: Study area map

The annual ultraviolet (UV) index is 9.3 with an average cloud cover of 5% annually. The temperature, UV index and cloud cover combination are indicative of high solar energy potential. Braamfontein is in the highveld region of Gauteng and hence receives high solar radiation compared to surrounding areas. The haphazard distribution of building heights on campus results in significant shadowing effects which lower solar radiation exposure to the low-rise building rooftops. Jacaranda and eucalyptus trees also contribute to shadowing as they are randomly located in the campus built-up area.

3.3 Data analysis

3.3.1 Area solar radiation calculation algorithm

The Solar Analyst Model (developed by Fu and Rich) was used to calculate the incoming solar radiation reaching the rooftops, because of its applicability at both regional and local scales. The Area Solar Model creates an upward hemispherical viewshed for every point within the DSM. The model searches in a specific set of directions to calculate a viewshed based on the maximum obstruction angle/horizon angle in every direction. The obstruction angle is then converted to a hemispherical coordinate system. The grid cell viewshed is identified in the obstructed or visible sky directions. These angles are used to divide the sky into a series of sectors. The resultant viewshed map, sun map and sky maps are overlayed repeating the process for all locations to produce the incoming solar radiation map as illustrated in the 1methodology flow diagram in Figure 2

To deal with variations in exposure due to the sun, the site area latitude was considered in the model as it represented solar declination and solar position. The sunmap is a representation of position of the sun over time. The sun track for each cell depends on the location and the time of day and year. When calculating direct radiation, the tool determines whether the sky is visible or obstructed for each cell in this surface grid, it identifies the solar constant, transmittivity, time duration, the portion of visible sun, and the angle of incidence (Esri 2013a To add on, solar radiation calculation was done separately for winter and summer months due to the flexibility of configuring the model to any time scale.

The total solar radiation is calculated by summing direct insolation (I_{dir}) obtained from the sun map sectors. Mathematically this can be expressed as shown in Equation 1:

$$\mathbf{R_{dir} = \sum I_{dir} = \sum S_{const} * \beta^{m(\theta)} * T_{\theta,\alpha} * G\alpha\rho_{\theta,\alpha} * \cos(I_{\theta,\alpha})} \qquad \textbf{(Equation 1)}$$

- S const = solar flux outside the atmosphere. In this case, it is 1.37 W/m^2 as specified by the world Radiation Centre Standard.
- β = mean transmissivity of the atmosphere.
- $^{m(\theta)}$ = optical path length.
- $T_{\theta, \alpha}$ = sky sector time duration.
- $G\alpha\rho_{\theta,\alpha}$ = sun map gap fraction sector.
- $I_{\theta, \alpha}$ = angle of incidence between the axis and centroid of the sky.

The effect of surface orientation is measured by multiplying the cosine of the incidence angle (ESRI, 2021). The incidence angle $I_{\theta, \alpha}$ is calculated as shown in Equation 2:

$$\mathbf{I\theta\alpha = acos\ (cos\ (\beta) * cos\ (G_Z) + sin\ (\theta) * sin\ (Gz) * cos\ (\alpha - G_a)} \qquad \textbf{(Equation 2)}$$

- G_Z is the zenith surface angle.
- G_a is the azimuth angle.

The total diffuse solar radiation for the location (R_{dif}) is calculated as the sum of diffuse solar radiation (I_{dif}) configured in the time interval corrected by the gap fraction and angle of incidence as shown in Equation 3:

$$\mathbf{R_{dif} = R_{glb} * P_{dif} * T_{dur} * SkyGap_{\theta,\alpha} * W_{\theta,\alpha} * cos(I_{\theta,\alpha})} \qquad \textbf{(Equation 3)}$$

- R_{glb} = the global normal radiation.
- P_{dif} = the proportion of diffused global radiation flux which is 0.3 for a clear sky
- T_{dur} = the time interval for the analysis.
- $W_{\theta, \alpha}$ = diffused radiation in proportion to the other sectors.
- $I_{\theta, \alpha}$ = incidence angle between the centroid of sky sector and the intercepting surface.

3.3.2 Spatial description of solar radiation maps

Using the above model, radiation maps were analysed (See the results in Chapter Four) to determine the spatio-temporal variation of solar radiation across the study area from 2019 to 2021. Daily solar radiation maps were computed together with a three-year cumulative solar radiation map for the period January 2019 to December 2021. The map units were in kilowatt-hours per square metre (kWh/m^2). The output solar radiation maps allow for the visualisation of solar radiation distribution across rooftops for each campus building. Analysis was done to determine if there are any significant differences between incoming solar radiation in summer versus winter months. It is important to note that the model considers the shape of the buildings,

shade caused by nearby trees and other urban elements which may affect the distribution of solar radiation.

3.3.3 Calculation of power potential per building

To calculate the power potential per building, the solar radiation cells were aggregated to their respective buildings in the building footprint shapefile. The average annual solar radiation raster was generated by configuring the model to calculate the cumulative solar radiation from 2019 to 2021. The rooftop area for each building was multiplied by the average solar radiation per square metre and the resultant raster layer was represented as the cumulative average solar radiation from 2019 to 2021. To convert the solar radiation to electricity potential, Equation 4 below was applied incorporating solar panel efficiency and the installation performance ratio. This is because these two factors significantly affect the electricity output.

Solar radiation * 0.16*0.86 = Total generated energy per building (megawatt per hour) (Equation 4)

Monocrystalline solar panels are regarded to have a conservative best estimate of at least 16% solar panel efficiency and 86% solar panel performance ratio (Palleries et al 2006). This implies that solar panels convert 16% of incoming solar radiation into electricity and 86% of this is preserved as it goes through installation. Calculation of the power potential was done for all buildings. However, to minimise the number of rooftop solar panels to achieve cost-efficiency and minimised visual impacts, it is necessary to only install them on the roof cells which receive the most solar radiation. To achieve this, a suitability criteria was applied to identify roof cells which have maximum exposure to solar radiation.

Some of the suitable cells appear to overlap from the rooftop outline, as shown on the suitable cells map. This is because the map was zoomed in to enable better visualisation in the print composer which resulted in the expansion of pixels.

3.4 Identifying the most suitable site for installation of solar panels

3.4.1 Suitability analysis

a) Suitability analysis criteria

The above calculation was used to calculate the power potential for all the buildings on campus. Three factors were used in this study to extract only the rooftop cells (suitable area cells) which receive high insolation. These factors were the average annual solar radiation, slope and rooftop orientation. Both the slope and aspect layers were calculated from the DSM.

b) Slope

The DSM was used to generate the slope layer. The range of the slope values is 0 degrees for horizontal roofs up to 90 degrees for vertical roofs. The rooftop slope is an important factor which limits and determines the solar panel tilt angle. The solar panel performance is strongly affected by its position relative to the sun. The electricity generation potential is highest when the incidence angle of the sun angle is perpendicular to the panel. It is assumed that the tilt angle is determined by the latitude of the area. In high latitude areas (where there are more sunlight hours in summer than winter), the solar panel tilt should be optimised for summer seasons. However, in this research, there was no significant difference in UV index between winter and summer. (Hong et al.2017) concluded that the tilt angle is negligible, and all panels should be placed horizontally on the rooftops. For this reason, the rooftop slope chosen to be suitable was between 60 and 90 degrees (slightly tilted to flat).

c) Orientation

Suitable orientation ensures maximum exposure to the sun annually. Thus, suitable rooftop cells in the context of Wits University (in the southern hemisphere) are those which are north facing as they receive the maximum solar radiation. The spatial analyst tool was used to derive aspect values from the DSM.

d) Average annual solar radiation

Suitable rooftop cells were classified as those that receive above-average solar radiation determined by the cumulative annual solar radiation map. The average value was 0.26 kWh/m^2.

3.4.2 Assessment of solar panel efficiency using land surface temperature

Past studies have used land surface temperature as an indicator of solar panel efficiency (Hofierka, 2004). High temperature areas are associated with high solar panel efficiency while

low temperature areas indicate low efficiency. LST across the study area was retrieved using the Landsat 8 Operational Land Imager (OLI) thermal bands as shown in Figure 2.

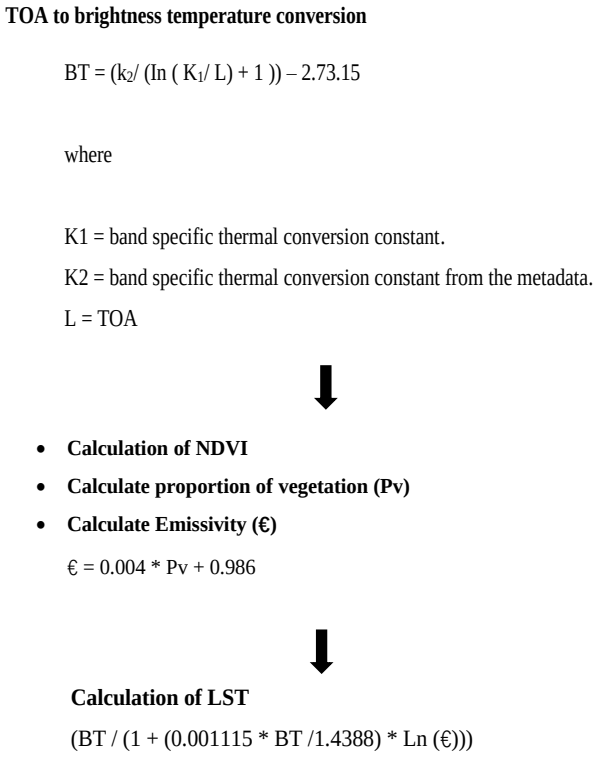

Figure 2: Flow diagram showing the stages in land surface temperature calculation.

However, to prove the relationship between LST and solar radiation, correlation and regression analysis was done on the two variables. Before carrying out these two tests, data normality test (Kolmogorov-Smirnov) was done on the datasets to determine their distribution and decide whether to use parametric or non-parametric tests for the correlation and which regression type to use. Descriptive statistics were used to analyse and quantitatively describe the LST and solar radiation datasets to derive basic information and identify potential relationships.

3.4.3 Sampling for solar radiation and LST correlation analysis

80 observations points were randomly selected for sampling of solar radiation and the corresponding LST reading as shown in the map below. Random sampling was done because every point in the study area had an equal chance of being selected hence reduced bias in the process.

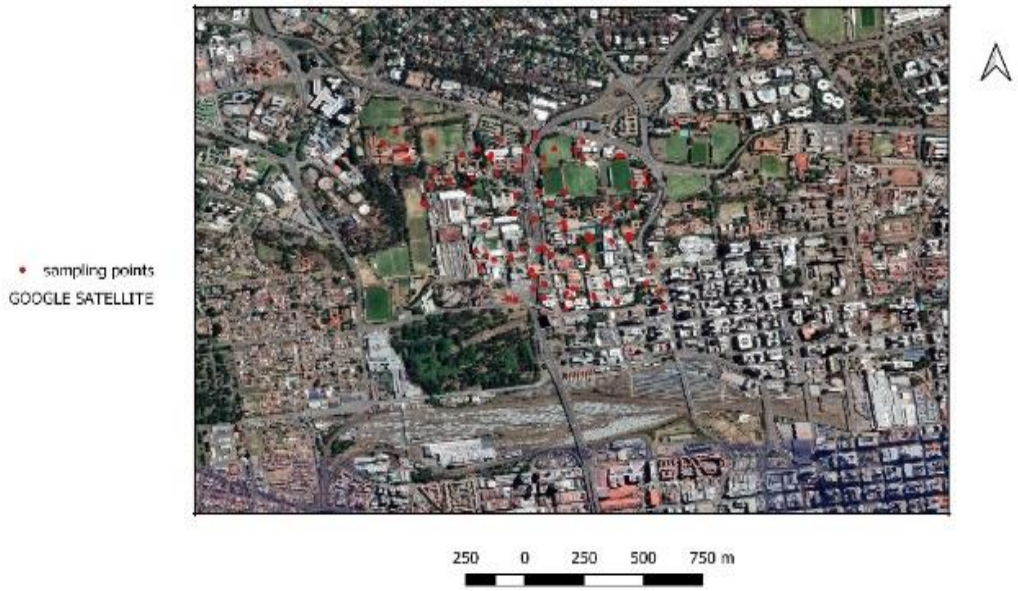

Figure 3: Map showing randomly selected sampling points for correlation analysis.

Figure 4: Summary of the research methodology used in the study describes the methodology used in this study for solar energy potential modelling and identification of suitable rooftop area size for the installation of solar panels for maximum power generation.

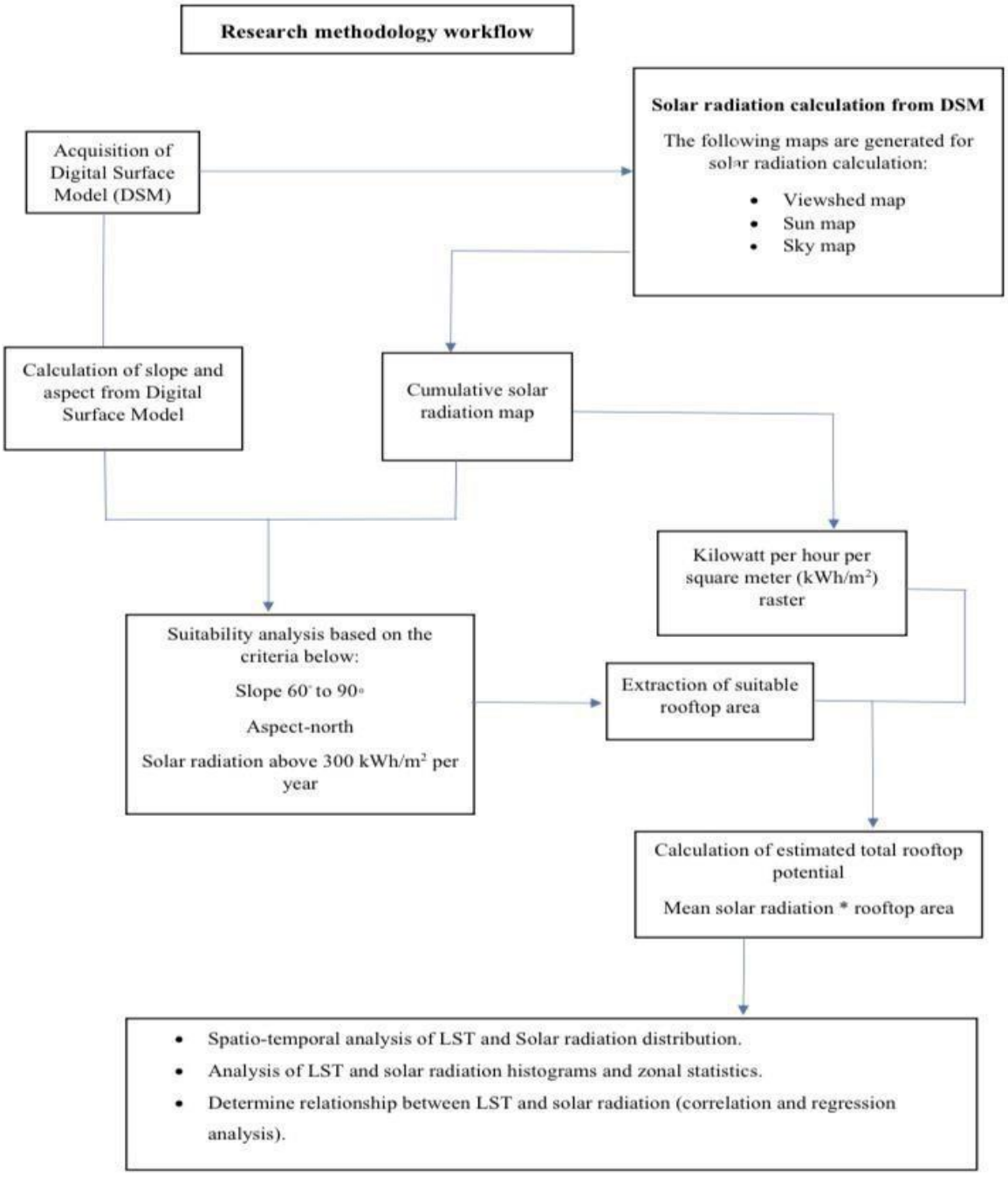

3.5 Data validation

To validate the solar radiation model used in this research, the information from the Global Solar Atlas was used. This is an online based global map which provides reports on the incoming solar radiation statistics for any location and temporal scale. These reports are suitable for validation purposes because they have a relative bias of +/−2.5 units according to ground measurement comparisons published in the SolarGIS Model Validation Report for the South African region. From 2019 to 2021, a maximum of two solar radiation maps per month were produced and the averages of these maps (derived from histograms) were compared to the SolarGIS average for the corresponding dates. The RMSE was used to assess the variation between the modelled and expected solar radiation averages. The RMSE measures the deviation of the modelled values from the measured values using the Euclidean distance. The formula for RMSE illustrated below was used:

RMSE= **(SQRT)** $\sum^{N}\mathbf{i = 1(x_1 - x_2)^2 \div N}$ **(Equation 6)**

Where:

- i is the variable (solar radiation)
- N is the number of observations
- x_1 is the actual observation value (ASR Model)
- x_2 is the estimated observation value (Solar GIS values)

RMSE values range from 0 to 1 where low values indicate that the LST algorithm calculated the temperature values accurately while high values represent low accuracy.

The same RMSE method was applied to validate land surface temperature. The temperature dataset averages were compared to those on GIOVANNI (Goddard Earth Science Data and Information Services Centre) Interactive Online Visualisation and Analysis Infrastructure. This is an online platform for exploring, analysing and comparing remotely sensed climatic datasets using a web browser (Acker et al., 2005).

The University of Witwatersrand campus map and field observations were compared to the Google Earth imagery to ensure that buildings were not omitted and to match the names to those on East and West campus.

3.6 Data analysis

Results for solar energy spatial distribution were analysed as spatio temporal distribution maps. Daily solar radiation trends were plotted in a time series analysis to observe annual daily patterns. Solar radiation descriptive statistics analysis including daily averages, standard deviation and variance was done to quantitatively analyse solar radiation distribution values. Correlation analysis was done between LST and solar radiation to establish the relationship between these 2 variables. Validation for solar radiation and temperature values was done using the Root Mean Square Error. There was a strong correlation between observed and modelled values for both solar radiation and LST.

CHAPTER 4: RESULTS

4.1 Solar radiation daily spatial distribution

The map below shows the spatial distribution of daily average solar radiation across building rooftops from 2019 to 2021. The maximum observed daily radiation was 6 kWh/m^2 and the minimum was 0.00002 kWh/m^2. The solar radiation distribution shown below in Figure 4 shows radiation trends on rooftops before the suitability criteria were applied.

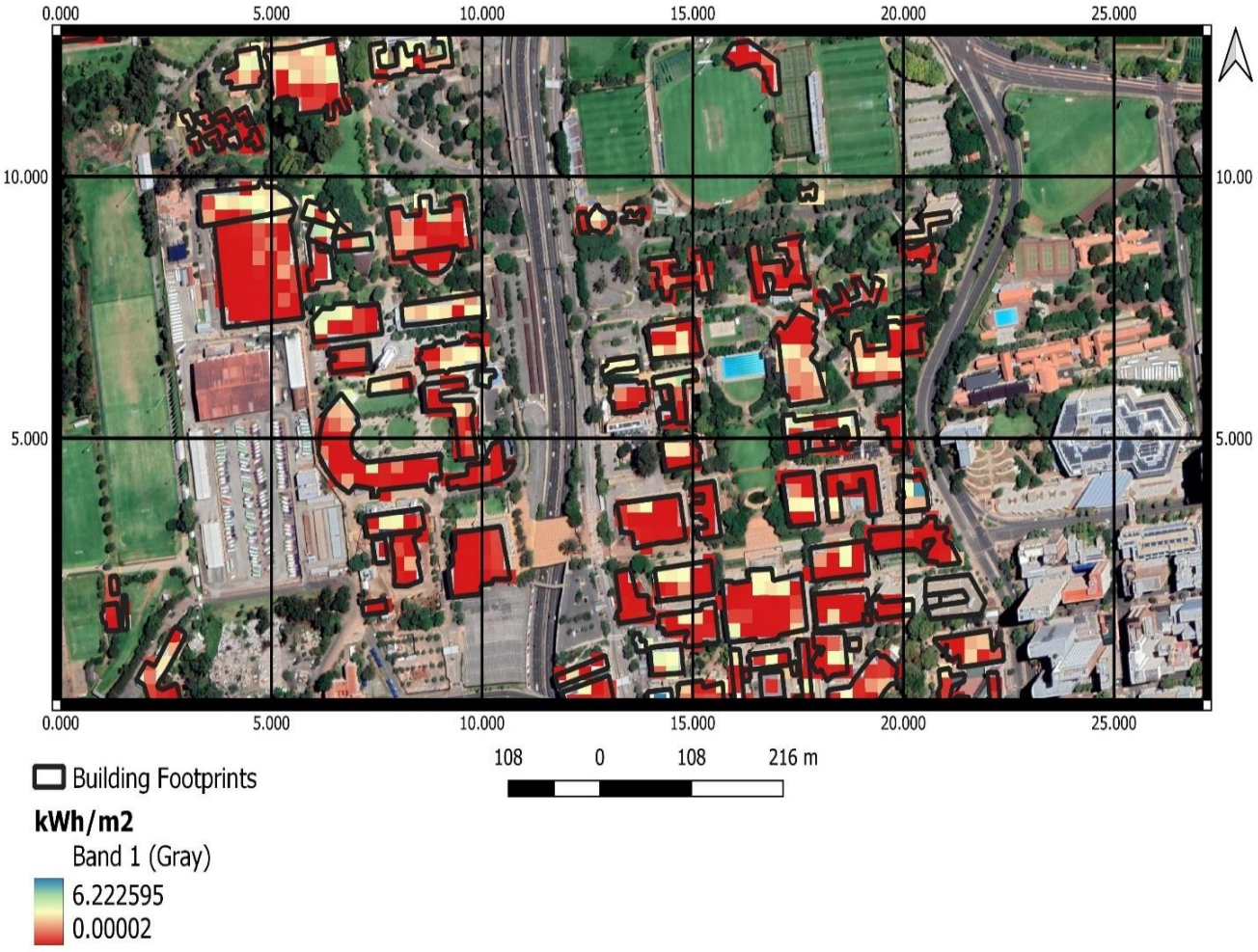

Figure 5: Map showing Average Daily solar radiation for the period 2019 to 2021. Radiation was measured for all the building rooftops across campus.

4.2 Daily spatio-temporal solar radiation distribution across East and West Campus

To assess the daily solar radiation trends across the study area, 39 maps were generated for specific days throughout each month of the year. The solar radiation spatial distribution appeared to be random throughout the year and no anomalies were observed. There was no notable difference in solar radiation values between winter and summer months. To

quantitatively analyse the maps, a plot showing maximum and minimum solar radiation values was computed as shown below.

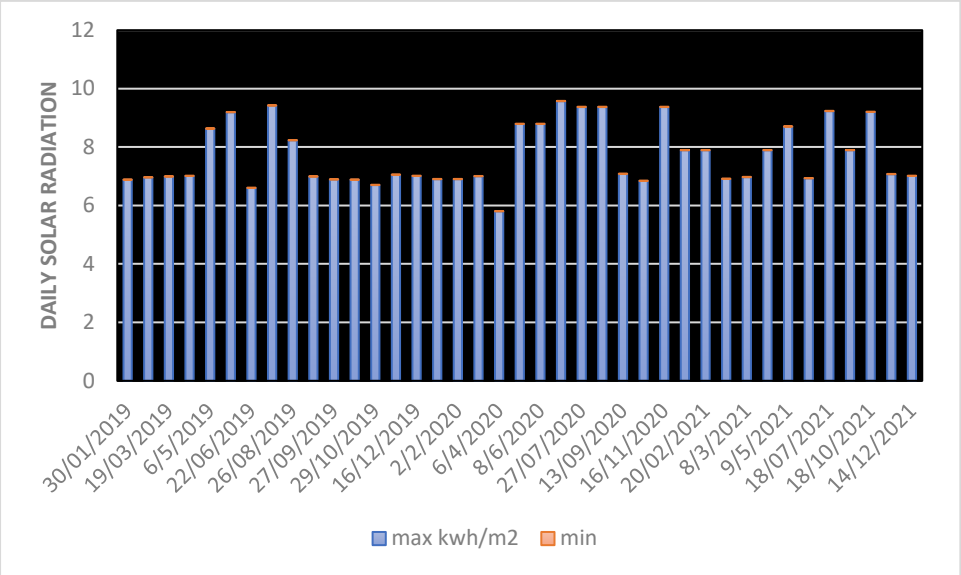

Figure 6: Solar radiation distribution statistics

4.3 Solar radiation distribution quantitative analysis

The column chart above shows the maximum and minimum daily solar radiation distribution derived from solar radiation maps for specific days of each month from 2019 to 2021. Across the study area, above 80% of the pixels fell between 2 to 6 kWh/m^2 daily which is within the SolarGIS daily recorded average for the region of South Africa. The median is 5 kWh/m^2; hence 50% of the radiation values fell below this value and the other 50% above the value. The frequency of values above 10 kWh/m^2 was low which is an indication that all values above 10 kWh/m^2 were anomalies. The standard deviation is 3 indicating that there is low variability of solar radiation between summer and winter months.

To identify rooftop cells with the highest generation capacity, suitability criteria were applied based on slope, aspect and solar radiation intensity. This resulted in low solar radiation (unsuitable) rooftop cells being removed as shown in Figure 7 below. This is important for ensuring that solar panels are installed on maximum generation capacity rooftop sites.

4.4 Suitability analysis results

The map in Figure 7 shows the annual generation capacity based only on suitable rooftop area. The maximum solar radiation recorded was 2 342 kWh/m^2. All the suitable cells had above-average generation capacity with a minimum of 328 kWh/m^2.

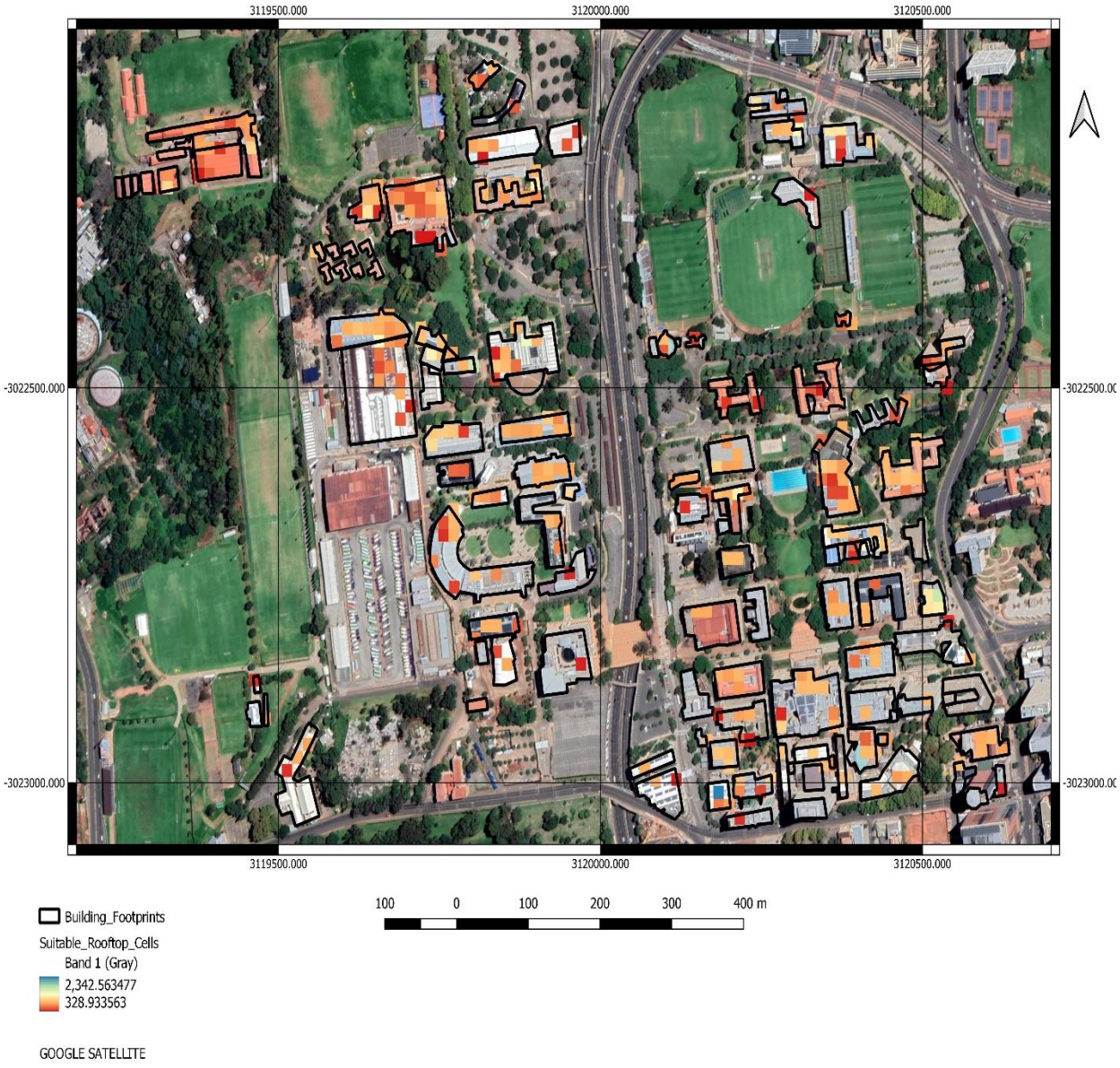

Figure 7: The annual generation capacity in kWh/m^2 based on multiplying only the suitable rooftop area by the energy available per square metre. Only the suitable rooftop sites for solar panels installation are shown.

4.5 List of buildings and three-year cumulative generation capacity (2019 to 2021)

Table 1 provides the list of buildings at University of Witwatersrand (Wits University) and their respective cumulative generation capacity over the study period.

Table 1: Suitable area for solar panel installation and the total electricity produced for 2019 to 2021 for each building at Wits University. The buildings highlighted in red are unsuitable for solar panel installation as they generate the least energy.

OBJECT ID *	Building name	Rooftop area	Mean kWh/m^2	Electricity produced (megawatts per hour)
1	Sh6	1504,933771	362,524418	581,1766532
2	Schonland Research Centre	1289,943233	318,044941	567,8192901
4	Solomon Mahlangu	1289,943233	347,141795	1777,865521
6	Richard Ward	1719,92431	474,304848	1024,287486
7	Paleo Science Building	644,971616	1271,963806	70,98946198
8	Faculty of Commerce Law and Management	1934,914849	745,655344	363,2885904
9	Du Plessis Centre	10104,55532	156,367197	9046,895847
10	Wits Sports	3224,858082	223,925274	2016,208905
11	Chalst Centre	859,962155	145,815799	825,6629427
12	Wits Club	859,962155	557,517773	215,9477375
13	The Barns	859,962155	143,350608	839,8618142
14	John Orr Engineering School	4084,7765	124,149872	2652,554636
15	Bidvest Wits Training Facilities	2000	500	2690,098
16	PIMD	214,990539	785,8396	38,30129642
17	Wits Planetarium	1006,987	688,987	1216,5698
18	Auditorium	859,962155	17,550307	6859,976962
19	Admin and Oliver Sheimer	2364.89592	3152.589958	427.6479308
20	Biology	2364,895927	215,628815	1535,441494
21	Cals Centre for Applied Science	3224,858082	609,70809	740,4857158
22	CCDU	2149,905388	77,554708	3880,960448
23	CLTD	429,981078	7,537918	7985,93868
24	Sunnyside Residence	4514,801314	414,382069	1525,336715
25	Wits Development Hub	2579,886465	422,551248	854,7699405
26	Chamber of Mines	4084,820237	80,182516	7132,16374
27	David Webster Hall	1934,914849	705,584533	383,9200921
28	Digi	1074,952694	665,568734	226,1124501
29	Flower Hall	1719,92431	182,864237	1316,765964
30	Great Hall and R. Sobukwe	5589,754008	326,779985	2394,778129
31	Gemini Lab	1289,943233	503,663595	358,5568908
32	Hall 29 Extension	2794,877004	258,914042	1511,245885
33	Wits Theatre	2364,895927	323,277233	1024,153253
34	Emthonjeni Centre	1074,952694	1053,593164	142,8382248
35	Wits Arts Museum	429,981078	193,496119	311,1036605
36	Student Corner	644,971616	401,951085	224,6443152
37	Gatehouse	859,962155	239,288597	503,1359756
38	Humprey Rakes	1934,914849	101,425099	2670,818974
39	Wits School of the Arts	2364,895927	600,42923	551,4145768
40	Oppenheimer Life Sciences	3869,829698	92,285104	5870,678303
41	Faculty of Commerce Library	1289,943233	195,808442	922,2894109

42	Hofmeyr House	644,971616	35,737236	2526,66508
43	International House	1504,933771	192,80712	1092,753877
44	Chris Hall	644,971616	88,794691	1016,907939
45	Physics	2364,895927	287,895141	1150,020902
46	Wartenweiler Library	1934,914849	271,0252	999,494065
47	Jan Smuts House	1074,952694	0,954566	157656,3351
48	Socio-Eeconomic Rights Institute	1719,92431	525,664689	458,0665364
49	Umthombo	1074,952694	502,752388	299,3389604
50	The Matrix	3654,839159	498,658552	1026,107905
51	College House	2579,886465	127,094502	2841,854678
52	Dairmpie House	1934,914849	140,005333	1934,841145
53	Jubilee	644,971616	677,560598	133,2663477
54	Bozzoli Sports Pavilion	1504,933771	57,227469	3681,636312
55	The Sanctuary	214,990539	629,41333	47,82020657
56	Wits Multi-Purpose Hall	2364,895927	387,735123	853,8958947
57	School of Architecture	1074,952694	121,941658	1234,142455
58	John Moffatt	1504,933771	638,152464	330,1573524
59	William Cullen	1289,943233	301,974685	598,0370594
60	Geosciences	1289,943233	7,378105	24476,75285
61	Northwest Engineering	3224,858082	141,369267	3193,622921
62	Bernard Price	859,962155	785,101597	153,3491998
63	Solomon Mahlangu	644.971617	518.181091	422.2794
64	Southwest Engineering	2364,895927	316,831535	1044,988876
65	Hillman	2149,905388	265,264693	1134,665722
66	Origins Centre Prehistory	859,962155	227,665369	528,8230802
67	Wits Origin Centre	2149,905388	214,190963	1405,226206
68	Locker Room	644,971616	795,670431	113,4842049
69	TW Kambule	2794,877004	232,895264	1680,080453
70	Old Grandstand	859,962155	576,651065	208,782588
71	Wits Law Clinic	2149,905388	510,568324	589,5131761
72	New Commerce Building	1934,914849	589,687249	459,375846
73	West Campus Cluster	1719,92431	152,014103	1583,993844
74	Squash	1289,943233	247,595694	729,3828487
75	Barnato	5589,754008	465,647028	1680,598209
76	Convocation	1289,943233	773,823868	233,3761727
77	School of Accounting	4729,791853	387,518506	1708,746419
78	High Voltage Building	214,990539	1,887276	15948,21079
79	Wits Plus	214,990539	1108,524292	27,15202155
80	Wits Science Stadium	6019,735086	218,718984	3853,176787

4.6 Spatio-temporal distribution of land surface temperature

Descriptive statistics below were used to quantitatively analyse the distribution of LST. The daily average temperature was found to be 22.92 °C, with a standard deviation of 6.91 °C which is high, indicating high variation of temperature across the study area. The highest temperature range was 24 °C to 30 °C.

To derive the relationship between land surface temperature and solar radiation, LST distribution maps were generated, matching the solar radiation maps' dates (see Figure 8). To confirm if LST can be used as an indicator of solar radiation potential, correlation and regression analysis was done on these two variables.

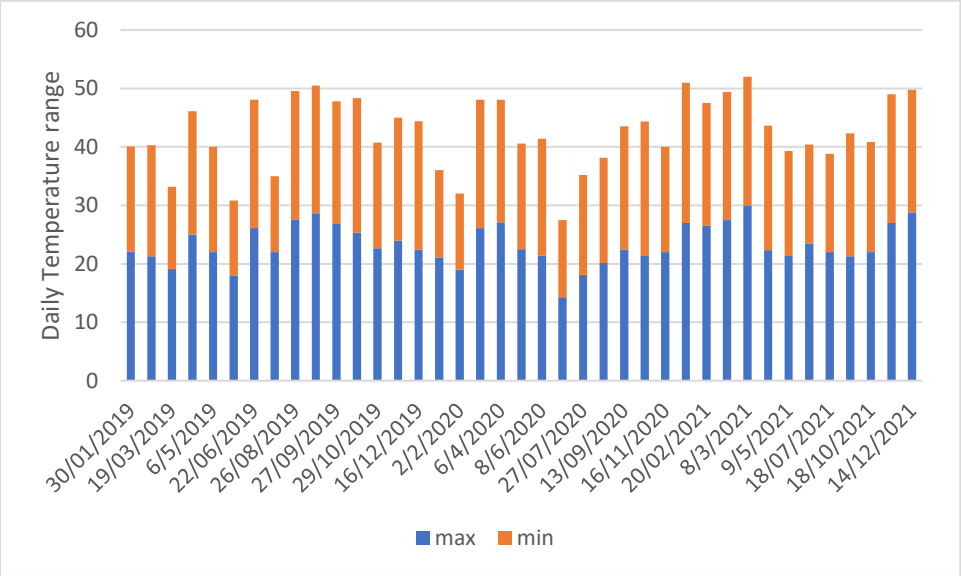

Figure 8: LST distribution maps

4.7 Correlation analysis: Solar radiation versus solar radiation intensity

To measure the strength of relationship between LST and solar radiation, Spearman correlation analysis was done as shown in Figure 9. This was important to determine if LST affects solar panel efficiency. The Spearman correlation is appropriate because datasets of the two variables follow different distributions (random and non-random).

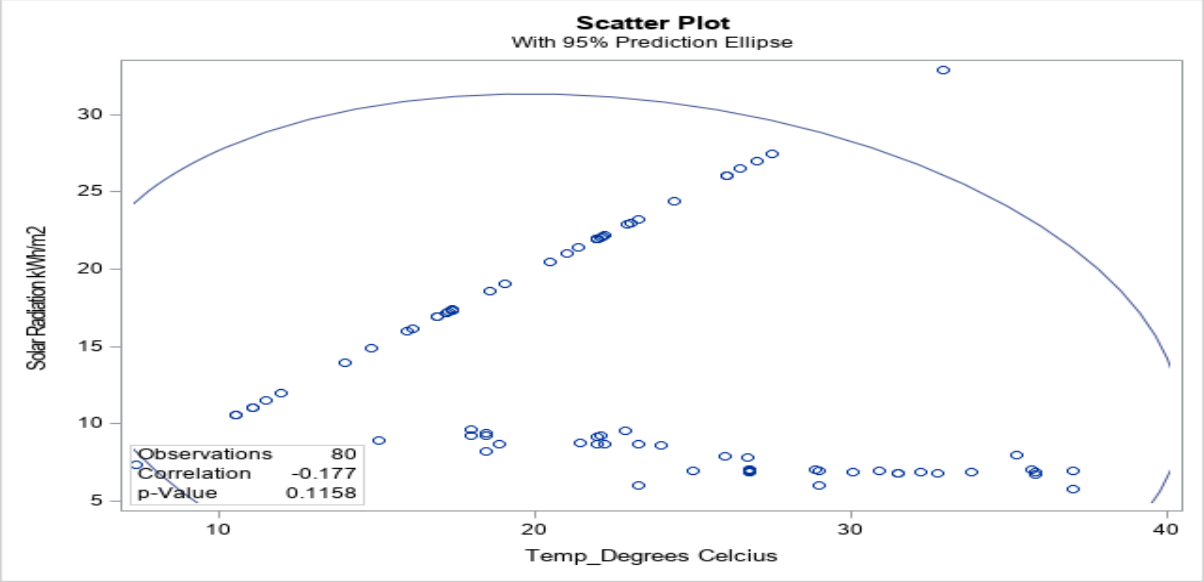

Figure 9: Correlation analysis between solar radiation and LST.

Null Hypothesis: There is no correlation between solar radiation and LST.

Alternative Hypothesis: There is correlation between solar radiation and LST.

The correlation coefficient was −0.177. This means that there was a negative 10.77% correlation between the two variables. This is a very weak correlation and indicates that the ratio of change between the variables is non-constant. The p value is 0.1158 which is greater than 0.05 (at 95% confidence interval); hence we fail to reject the null hypothesis which states that there is no correlation between the two variables. From this analysis, solar radiation intensity was not correlated to land surface temperature – hence LST cannot be used as an indicator of electricity generation capacity (see Figure 10) below.

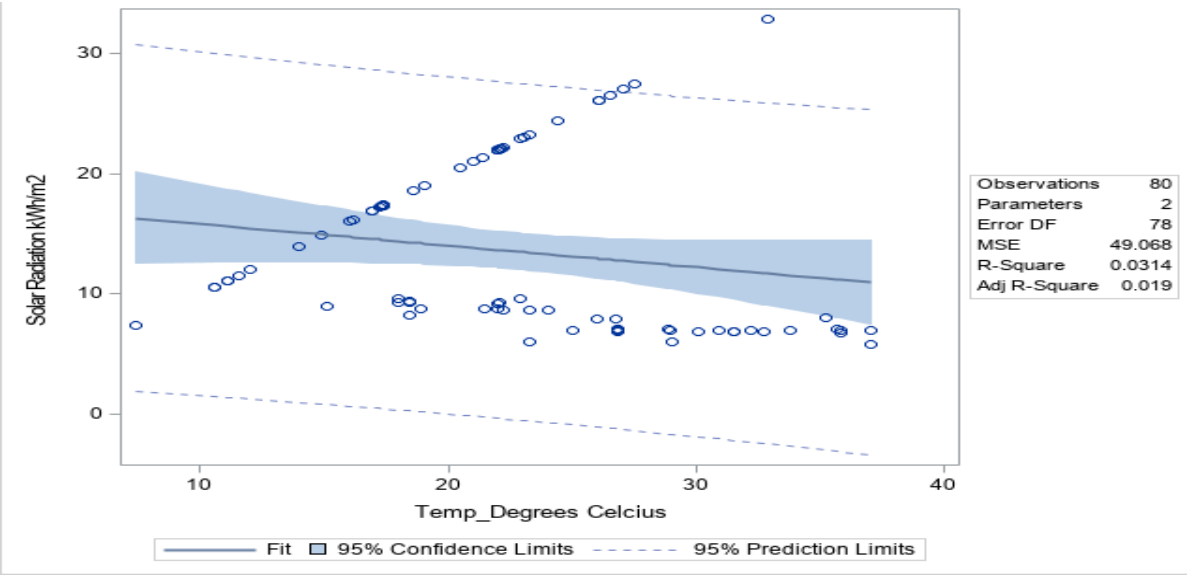

Figure 10: Linear regression model showing relationship between solar radiation and land surface temperature. The model does not fit the data which indicates that there is no relationship between the two variables.

4.8 Validation of solar radiation intensity and land surface temperature

To validate the modelled daily solar radiation, the daily values were compared to the SolarGIS daily reported values using the RMSE as shown in figure 11. The calculated RMSE was 0.15, which indicates that there is a 15% variation between modelled values and the actual solar radiation intensity. The variation was relatively low and could be a result of errors associated with the acquisition of remotely sensed data. From this analysis, the area solar radiation model was applicable to the study area with a low error margin.

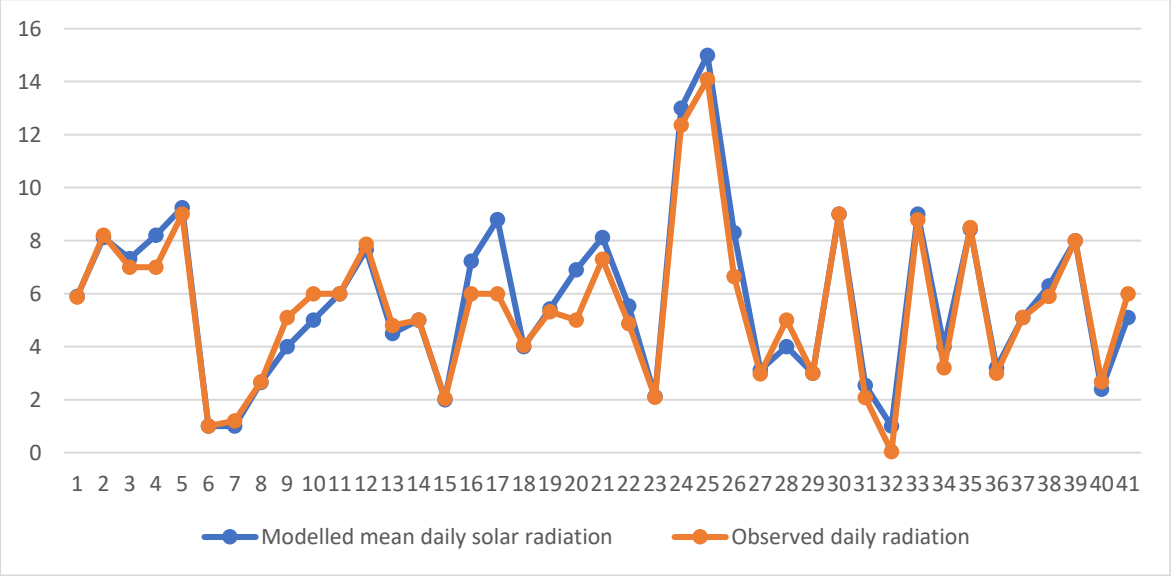

Figure 11: Plot showing modelled solar radiation against observed daily radiation.

To validate LST, the daily average modelled values (L8 OLI) were compared to the daily average from GIOVANNI and an RMSE of 0.13 was obtained. This implies a 13% variation between the modelled values and actual temperature measurements. This variation is relatively low; hence Landsat 8 can be used with accuracy to model land surface temperature. Table 2 shows the daily solar radiation values and land surface temperature values compared against validation datasets (SolarGIS and GIOVANNI).

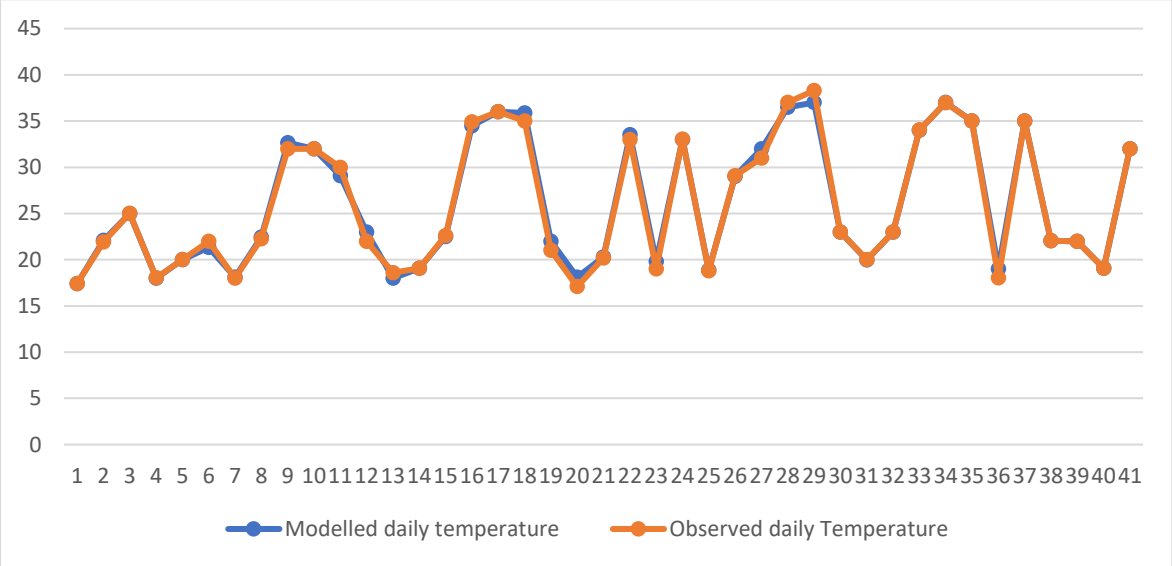

Figure 12: Observed and modelled LST values were compared using the RMSE to evaluate the accuracy of data.

CHAPTER 5: DISCUSSION AND CONCLUSION

Discussion

5.1.1 Daily solar radiation and annual spatial distribution

The daily average solar radiation was 5 kWh/m2 which does not substantially deviate from the SolarGIS daily solar radiation value of 6 kWh/m2 for Johannesburg. The standard deviation was 3.32 which indicates a moderately high variation of solar energy distribution considering the study area extent. No notable differences between summer and winter solar radiation intensities were observed. The distribution of solar radiation values was heterogeneous as different solar radiation values were recorded on the same rooftops. The angle of incidence of the sun on every rooftop cell is different and this can account for the solar radiation variation at local scale. Further, uneven height distribution of the buildings across the university results in shadow effects which in turn obstruct solar radiation on low-rise buildings. Shading owing to the presence of trees also contributes to reduced solar radiation intensity.

5.1.2 Suitability analysis results

After carrying out the suitability analysis, all rooftop cells with low solar radiation were removed. The total rooftop area for all the buildings before suitability analysis was carried out was 157 588,0649 m^2. After the extraction of suitable cells, this area reduced to 58 907,40763 m^2. Based on the analysis in the present study, 93% of the buildings were classified as suitable while only five buildings (Paleo Science building, Chalst Centre, The Barns, Wits School of Arts and Chris Hall) were deemed unsuitable. Based on the rooftop area, the total generation capacity for all the buildings for the period 2019 to 2021 was 559 200 MWh. This calculation is based on the conservative best estimate of 16% solar panel efficiency as explained in Chapter Three (Methodology). Buildings with larger rooftops generally have a higher generation potential than smaller rooftops. The annual energy demand is above 60 GWh; hence energy from solar panels can meet the current demand. Results from previous research studies indicate that incoming radiation estimates may be inaccurate since they are influenced by weather conditions in this study, generation potential was calculated based on clear sky conditions and hence, generation capacity may be slightly lower than modelled values. There is no significant difference between winter and summer radiation trends in this study. In this study, conditional analysis, GIS techniques and remote sensing have proved their great potential for mapping the suitability of solar panel installations based on analysis of multiple factors affecting solar energy generation potential.

5.1.3 Significance of LST on solar panel efficiency

The distribution of LST across the study area was heterogeneous. The anomalies that were observed were randomly distributed throughout the year. LST has higher spatial variation compared to solar radiation intensity. This implies that there is no correlation between these two variables. In addition, values are dispersed from the regression line of fit which indicates no relationship between the variables.

5.2 Recommendations

The framework used in this study did not evaluate technical factors which affect site selection process for rooftop solar panel installation. Although the main factors affecting electricity generation capacity (solar radiation and shadow effects) are considered in this study, some factors (for example array solar height and space between the arrays) have not been incorporated in the GIS-based model. In other studies, additional roof reinforcement and roof load data were analysed. This was not considered since this study focused on only geophysical factors for rooftop site selection.

Improved sources of data incorporating other criteria would improve the selection of the solar panel mounting sites on campus. Calibrated and more accurate (high-resolution) DSMs are important in the modelling of incoming solar radiation and for the provision of rooftop footprint data.

However, there is a huge gap between the GIS solar radiation generated maps and the actual practical applicability in the solar energy system design by various social groups. Minimising this gap can be done by adding an economic aspect to the geospatial context which increases the practicability of the models.

5.3 Conclusion

This study presented a method for modelling the potential for rooftop solar energy at the University of the Witwatersrand. The Area solar radiation model is highly accurate and calculates topographic influences on insolation across local and landscape scales. The results confirmed that the university has high solar energy potential in both winter and summer months. To add on, 95 buildings were found to be suitable for solar panel installations as they receive above average solar radiation across the study area. Temperature was found to have an insignificant contribution to solar radiation trends. The maps generated in this study can be combined with other factors and incorporated into economic feasibility analysis.

REFERENCES

Al-Badi, A.H., Malik, A and Gastli, A. (2009) Assessment of renewable energy resources potential in Oman and identification of barriers to their significant utilization, *Renewable and Sustainable Energy Reviews*, vol. 13, no. 9, pp. 2734-2739.

Antonopoulos, I., Robu, V., Couraud, B., Kirli, D., Norbu, S., Kiprakis, A., Flynn, D., Elizondo-Gonzalez, S. and Wattam, S. (2020) Artificial intelligence and machine learning approaches to energy demand-side response, *Renewable and Sustainable Energy Reviews*, vol. 130, no. 18, pp. 108-109.

Asakereh, A., Soleymani, M. and Sheikhdavoodi, M.J. (2017) A GIS-based fuzzy-AHP method for the evaluation of solar farms locations Case study in Khuzestan province, Iran, *Solar Energy*, vol. 155, no. 23, pp. 342–353.

Avtar, Y., Sahu, P., Aggarwal, D., Chakraborty, C., Kharrazi, X., Yunus, C., and Kurniawan, P. (2019) Exploring renewable energy resources using Remote Sensing and GIS, *Resources*, vol. 8, no. 3, pp. 149-150.

Broesamle, H., Mannstein, H., Schillings, C. and Trieb, F. (2001) Assessment of solar electricity potentials in North Africa based on satellite data and GIS, *Solar Energy*, vol. 70, no. 2, pp. 11-12.

Clifton, J. and Boruff, B.J. (2010) Assessing the potential for concentrated solar power development in rural Australia, *Energy Policy*, vol. 38, no. 9, pp. 5272-5280.

Clerici, A., Perego, S., Tellini, C. and Vescovi, P. (2006) A GIS-based automated procedure for landslide susceptibility mapping by the conditional analysis method: the Baganza valley case study (Italian Northern Apennines), *Environmental Geology*, vol. 50, no. 7, pp. 941-961.

Domínguez , J., García Casals, X. and Pinedo Pascua, I. (2007) GIS approach to the definition of capacity and generation ceilings of renewable energy technologies, *Energy Policy*, vol. 35, no. 10, pp. 4879-4892.

Fluri, T.P. (2009) The potential of concentrating solar power in South Africa, *Energy Policy*, vol. 3, no. 13, pp. 5075-5080.

Gan, W.Q., Zhang, H.Y., Chen, B., Zhang, Z., Wu, J., Deng, L., Huang, Y., Yang, J.-F., Cui, J.J., Chang, J., Wang, C., Wu, J., Yin, S., Chen, W., Fang, C. and Yan, Y.H (2019) Advanced space-based solar observatory (ASO-S), *Research in Astronomy and Astrophysics*, vol. 19, no. 11, pp. 156-157.

Gharakhani, S. and Pillay, P. (2012) Study of optimum tilt angles for solar panels in different latitudes for urban applications, *Solar Energy*, vol. 86, no. 6, pp. 1920-1928.

Gunerhan, H. and Hepbasli, A. (2007) Determination of the optimum tilt angle of solar collectors for building applications, *Building and Environment*, vol. 42, no. 2, pp. 779-783.

Guo, S. and Hussein, K. (2020) Materials for solar powered water evaporation, *Materials Today Energy*, vol. 12, no. 7, pp. 12-15.

Haurant, P., Oberti, P., and Muselli, M. (2011) Multicriteria selection aiding related to photovoltaic plants on farming fields on Corsica Island: case study using the ELECTRE outranking framework, *Energy Policy*, vol. 39, no. 2, pp. 676–688.

Huang, J. (2022) 'Wits' infrastructure and sustainability, *Campus Business Continuity Considerations in the National Electricity Crisis*, vol. 13, no. 34, pp. 8-9.

Hussein, K. (2001) Identifying and delineating thermally active areas in Colorado using thermal remote sensing data, *Research in Astrophysics*, vol. 31, no. 4, pp. 23-36.

Jochem, A., Hofle, B., Rutzinger, M. and Pfeifer, N. (2009) Automatic roof plane detection and analysis in airborne lidar point clouds for solar potential assessment, *Sensors*, vol. 9, no. 7, pp. 5241-5262.

Joseph, P., Roser, B.C., Marsal, L.F. and Schropp, R.E. (2006) A compact equivalent circuit for the dark current-voltage characteristics of nonideal solar cells, *Journal of Applied Physics*, vol. 100, no. 8, pp. 102-103.

Kylili, A., Fokaides, P.A., Ioannides, A. and Kalogirou, S. (2018) Environmental assessment of solar thermal systems for the industrial sector, *Journal of Cleaner Production*, vol. 1, no. 76, pp. 99-109.

Keleş, S. and Bilgen, S. (2012) Renewable energy sources in Turkey for climate change mitigation and energy sustainability, *Renewable and Sustainable Energy Reviews*, vol. 16, no. 7, pp. 5199-5206.

Kalogirou, S.A. (2001) Artificial neural networks in renewable energy systems applications, *Renewable and Sustainable Energy Reviews*, vol. 5, no. 4, pp. 373-401.

Kumar, C., Singh, S., Gupta, M.K., Nimdeo, Y.M., Raushan, R., Deorankar, A.V., Kumar, T.M.A., Rout, P.K., Chanotiya, C.S., Pakhale, V.D. and Nannaware, A.D. (2023) Solar energy: a promising renewable source for meeting energy demand in Indian agriculture applications, *Sustainable Energy Technologies and Assessments*, vol. 55, no. 13, pp. 102-105.

López, G., Batlles, F.J. and Tovar-Pescador, J. (2005) Selection of input parameters to model direct solar irradiance by using artificial neural networks, *Energy*, vol. 30, no. 9, pp. 1675-1684.

Menyah, K. and Wolde-Rufael, Y. (2010) Energy consumption, pollutant emissions and economic growth in South Africa, *Energy Economics*, vol. 32, no 6, pp. 1374-1382.

Mubiru, J. and Banda, E.J.K.B. (2008) Estimation of monthly average daily global solar irradiation using artificial neural networks, *Solar Energy*, vol. 82, no. 2, pp. 181–187.

Ningshen, P. and Mittal, H. (2016) GIS and Remote Sensing techniques for solar hotspots installation, *Mechanical Engineering International Journal*, vol. 3, no. 18, pp. 1-12.

Mutavhatsindi, T., Sigauke, C. and Mbuvha, R. (2020) Forecasting hourly global horizontal solar irradiance in South Africa using machine learning models, *IEEE Access*, vol. 8, pp. 198-199.

Pohekar, S.D. and Ramachandran, M. (2004) Application of multi-criteria decision making to sustainable energy planning, *Renewable and Sustainable Energy Reviews*, vol. 8, no. 4, pp. 365-381.

Popp, A., Dietrich, J.P., Lotze-Campen, H., Klein, D., Bauer, N., Krause, M., Beringer, T., Gerten, D. and Edenhofer, O. (2011) The economic potential of bioenergy for climate change mitigation with special attention given to implications for the land system, *Environmental Research Letters*, vol. 6, no. 3, pp. 134-135.

Rogelj, J., Luderer, G., Pietzcker, R.C., Kriegler, E., Schaeffer, M., Krey, V. and Riahi, K. (2015) Energy system transformations for limiting end-of-century warming to below 1.5 °C, *Nature Climate Change*, vol. 5, no. 6, pp. 519-527.

Staffell, I., Scamman, D., Velazquez Abad, A., Balcombe, P., Dodds, P.E., Ekins, P., Shah, N. and Ward, K.R. (2019) The role of hydrogen and fuel cells in the global energy system, *Energy and Environmental Science*, vol. 12, no. 2, pp. 463-491.

Soares, P.M.M., Brito, M.C. and Careto, J.A.M. (2019) Persistence of the high solar potential in Africa in a changing climate, *Environmental Research Letters*, vol. 14, no. 12, pp. 124-136.

Talut, M., Bahaj, A.S. and James, P. (2022) Solar power potential from industrial buildings and impact on electricity supply in Bangladesh, *Energies*, vol. 15, no. 11, pp. 4037-4038.